IEEE Access
Multidisciplinary ⋮ Rapid Review ⋮ Open Access Journal

Received May 14, 2020, accepted June 11, 2020, date of publication June 17, 2020, date of current version June 30, 2020.

Digital Object Identifier 10.1109/ACCESS.2020.3003035

Exploring Low Loss and Single Mode in Antiresonant Tube Lattice Terahertz Fibers

JAKEYA SULTANA[1], MD. SAIFUL ISLAM[1], (Member, IEEE), CRISTIANO M. B. CORDEIRO[2], MD. SELIM HABIB[3], (Senior Member, IEEE), ALEX DINOVITSER[1], (Member, IEEE), BRIAN WAI-HIM NG[1], (Member, IEEE), AND DEREK ABBOTT[1], (Fellow, IEEE)

[1]School of Electrical and Electronic Engineering, The University of Adelaide, Adelaide, SA 5005, Australia
[2]Institute of Physics, University of Campinas, Campinas 13083-859, Brazil
[3]Florida Polytechnic University, Lakeland, FL 33805, USA

Corresponding author: Jakeya Sultana (jakeya.sultana@adelaide.edu.au)

This work was supported by the Australian Research Council (ARC) under Grant DP170104981.

ABSTRACT We propose and numerically analyze various hollow-core antiresonant fiber (HC-ARF) for operation at terahertz frequencies. We compare typical HC-ARF designs with nested and adjacent nested designs while analyzing performance in terms of loss and single-mode guidance of terahertz waves. With optimized fiber dimensions, the fundamental core mode, cladding mode, core higher-order modes (HOMs), and the angle dependence of adjacent tubes are analyzed to find the best design for low loss terahertz transmission. Analysis of the fiber designs shows that the nested tube-based antiresonant fiber exhibits lower transmission loss and superior HOM suppression, exceeding 140. The nested HC-ARF is feasible for fabrication using existing fabrication technologies and opening up the possibility of efficient transmission of terahertz waves.

INDEX TERMS Terahertz, antiresonant fiber, waveguide.

I. INTRODUCTION

Lying midway between the microwave and visible light, the terahertz spectrum offers significant potential in the field of sensing, security, label-free molecular detection, hybridization of DNA, pharmaceutical drug testing, spectroscopy and short-range high-speed communications [1]–[8]. However, the applications in practice are limited as most of the terahertz devices depend on free space for its transmission. Free space transmission of terahertz experiences many undesirable losses due to the coupling with atmospheric components that significantly reduce transmission efficiency. Different approaches have been demonstrated for the terahertz wave guidance, this includes metallic wires [9], metal-coated dielectric tubes [10], sub-wavelength fibers [11], porous fibers [12], [13], photonic band-gap and kagome hollow fibers [14], [15].

The metal waveguides were used initially; the finite conductivity of metals, however, limits their use. Moreover, inflexibility and surface roughness of metals have also limited their use [16]. Dielectric waveguides have come into attention and shown impressive results but high absorption loss of conventional dielectrics has reduced its impact [17]. Some polymers, on the other side, have reduced material absorption coefficients in the terahertz range. Topas, Zeonex, Teflon, and HDPE have low absorption coefficients and possess high thermal and chemical stabilities being an exciting choice for practical applications [18].

Polymer-based hollow-core fibers are considered as a suitable candidate for low loss terahertz transmission as the majority of the terahertz signal pass through the core and only a small portion propagates through the cladding. Furthermore, as the majority of the signal ($> 99\%$) propagates through the core, the light-matter interaction is high that is suitable for sensing. In 2008, Lu *et. al* proposed the first hollow-core kagome based microstructured fiber for low loss terahertz transmission [19]. Using 5.5 mm core, the waveguide structure was assembled using Teflon® and achieved a low attenuation constant of 0.002 cm^{-1}. It has been found that the first cladding layer dominates the modal characteristics of the fiber, while the other cladding layers have very little influence [19], [20]. A similar kind of Teflon® based terahertz microstructured waveguide was proposed by Vincetti *et al.* where numerical analysis show transmission spectra with alternating high and low-loss regions. The high loss region is due to the coupling between the

The associate editor coordinating the review of this manuscript and approving it for publication was Kin Kee Chow.

core and cladding modes, whereas tube diameter and thickness are responsible to modify the low loss transmission band [20]. The strut thickness has also a significant impact on transmission bandwidth, thin strut thickness increases the transmission bandwidth where the opposite happens with thicker samples. The core diameter of a hollow-core fiber has an impact on overall loss. As the core diameter increases, the transmission loss reduces however large core also responsible for the multimode operation. Therefore, careful engineering required to design the fiber geometry and choosing the dimensions to achieve a low loss in a single-mode operating region.

In order to regulate the modal properties and reduce the overall loss, several types of HC-ARF have been reported, this includes circular antiresonant tubes [22], [25], [28], [29], ice-cream cone shape negative curvature antiresonant tubes [30], elliptical antiresonant tubes [31], and nested antiresonant node-free fiber [32]. A Zeonex tube lattice fiber for terahertz transmission was demonstrated with 1 dB/m loss at less than 1 THz with 3.84 mm of core diameter, with a tube thickness of 0.378 mm [28]. Drawn PMMA pipes are manually stacked to have a flexible circular tube lattice terahertz fiber and the transmission properties are demonstrated for straight and bent fiber [25]. In 2018, a 3D printed polycarbonate-based antiresonant terahertz waveguide [31] achieved a low loss of 0.009 dB/cm (0.9 dB/m) at 0.36 THz at the expanse of flexibility, due to a wall thickness of 0.6 mm and a core diameter of 10 mm. However, the reported losses are still high, and therefore there is further scope to propose fibers with comparatively low transmission loss with broad transmission bandwidth.

The concept of the on-node single cladding layer and hexagonal hollow-core ARF was first proposed, analyzed, and experimented in the visible-infrared regime [33]. Sequentially, the simple structure of on-node cladding [33] was advanced to node-free negative curvature cladding pattern [34]–[40] to improve the fiber performance. Different fiber parameters including the number of cladding tubes [37], the gap between cladding tubes [39], [40], single nested tubes [35], double nested tube and position of nested tubes [41] were considered to analyze the transmission loss, bending loss, and higher-order mode suppression capability in the optical regime.

The ARFs have been widely investigated in the infrared and mid-infrared range. However, there are very few studies in the terahertz regime. In this manuscript, along with the impact of gap variation on five, six and seven-tube ARFs, we have focused on the constant gap and the impact of the constant gap on tube numbers. Especially in the case of a five-tube fiber, which is advantageous both in lower transmission loss and higher-order mode suppression, it is not discussed in the published terahertz fibers literature. We have analyzed five-tube ARF in-depth and compare the performance when the tube number is more than five and the adjacent antiresonant tube gap is constant. We carry out the observation on typical, nested, and adjacent nested hollow-core antiresonant fiber designs to determine the optimal waveguide structure for low loss and broad bandwidth terahertz transmission. The adjacent nested ARF is very new in terahertz and we have demonstrated that adjacent ARF shows closely similar loss characteristics to nested ARF with proper optimization. An extensive analysis of the fundamental core modes, higher-order modes, and bending loss is carried out to achieve the information on modal contents of the fibers. The goal is to achieve a suitable waveguide structure by engineering various fiber geometries, the number of antiresonant tubes, the antiresonant tube thickness, fiber core diameter, and the fiber outer diameter considering constant and variable tube gap.

II. FIBER GEOMETRY

Fig. 1 depicts the profile of HC-ARFs with three different cladding structures. The core diameter D_c is at the center of the fiber, with the antiresonant tubes of D surrounding the core. The gap, g between two adjacent tubes forms a node-free boundary around the core. Also, the Zeonex tube thickness, t predicts the first transmission spectra centered around 1 THz. Here gray and white colour indicate the dielectric material and air regions respectively. In all of our numerical investigations, we kept $D_c = 3$ mm, $g = 0.99$ mm and $t = 0.09$ mm constant. The node-free core boundary shows comparatively lower and smoother transmission spectra than the on-node core boundary [21], [23], [24].

A regular five-tube HC-ARF is shown in Fig. 1(a). The nested HC-ARF in which a small nested tube with inner diameter, d is shown in Fig. 1(b). Fig. 1(c) shows an adjacent HC-ARF in which two adjacent nested tubes are placed in each antiresonant tube. For manufacturing perspective, we include a very small indentation of $t/3$ in the numerical model where the thin wall contacts another surface [42], including where (i) the antiresonant tubes contact the inner jacket surface and (ii) the nested tubes contact the wall of antiresonant tubes.

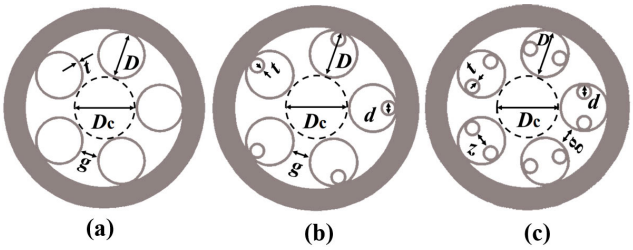

FIGURE 1. Cross-section of the fibers considered in simulations (a) Typical, (b) Nested, and (c) Adjacent nested HC-ARF. Here the optimum dimensions are $D_c = 3$ mm, $D = 2.1$ mm, $t = 0.09$ mm, $g = 0.99$ mm, and $d = 0.54$ mm.

A. FABRICATION POSSIBILITIES

The possible fabrication techniques for terahertz HC-ARF are stacking [25], [26], 3D printing [31] and extrusion [27]. The stack and drawn technique can collapse and deform the antiresoanat tube. To avoid this difficulty, the drawn

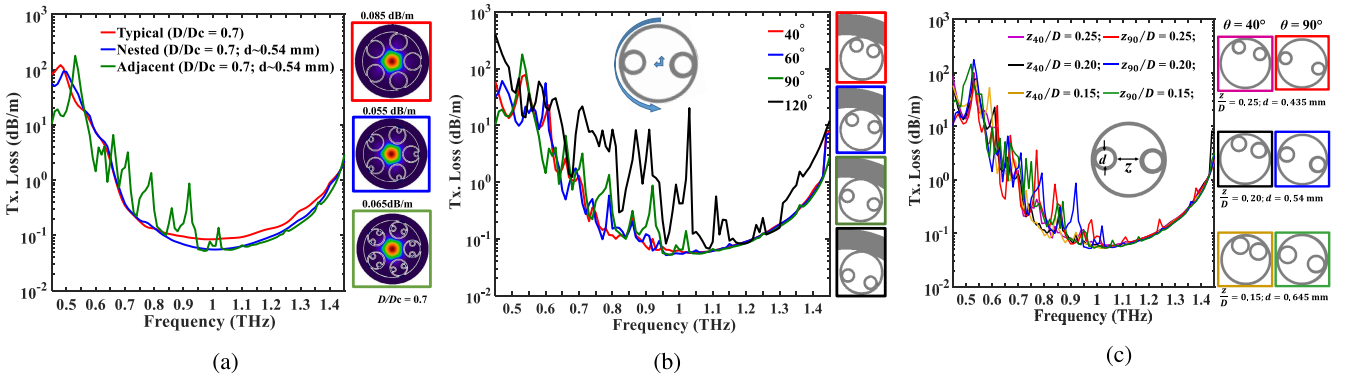

FIGURE 2. Transmission loss of five-tube based (a) typical, nested, and adjacent nested ARF; (b) adjacent nested ARF with different nested tube positions (θ); (c) adjacent nested ARF with different nested tube positions (θ) and different adjacent tube spacings (z/D). Here, $D_c = 3$ mm, and $t = 0.09$ mm.

antiresonant tubes are stacked manually inside the cladding jacket without any furnace. Although a flexible HC-ARF with thin dielectric strut is possible, the manual capillary stacking is very labour insensitive and time consuming procedure. The 3D printing technique is another suitable approach to fabricate the antiresonant tube with circular and complex configuration. The 3D printing technique is cost effective and easy to manufacture. However, this technique limits the strut thickness and fiber length. The extrusion technique where the HC-ARF can be fabricated directly from the melted granules. A metal die is placed at the nozzle of the extruder. The 3D metal printer can print the suitable metal die and the cross section of the metal die must be opposite to the geometry of proposed fiber. Extrusion technique is suitable for the desired strut thickness and long length fiber.

B. GUIDING MECHANISM OF HC-ARFs

In HC-ARFs, light is confined and guided to the air-core due to the weak coupling between core and cladding modes known as inhibited coupling [44]. A number of thin dielectric airy tubes around the air-core have lower refractive index than the core. Therefore, the low density of cladding mode guides light toward the core over a broad frequency range. Low loss region appears due to the inhibited coupling. However, in some narrow frequency ranges, the core mode couples strongly with cladding when the two modes are resonant and the transmission loss becomes high. The resonance frequency can be assumed from the thin dielectric wall using antiresonant reflecting optical waveguide (ARROW) model.

III. NUMERICAL RESULTS

The numerical investigations have been performed with finite-element method based COMSOL mode solver. Perfectly-matched layers (PML) has been used outside the fiber domain to calculate the leakage loss. Extremely fine mesh sizes are used in air and in the Zeonex walls for precise calculation.

A. FIVE-TUBE BASED HC-ARFs

Initially, the five-tube HC-ARFs with three different cladding patterns are taken in consideration to compare the transmission loss spectra and the fundamental mode profiles, presented in Fig. 2(a). In numerical calculations, the effective material loss estimated from the absorbed power in the Zeonex® struts are summed to the leakage loss in order to calculate the transmission loss. The solid red line indicates the transmission loss of a regular HC-ARF with a loss level of 0.085 dB/m at 1 THz. The solid blue line is the transmission loss of the nested HC-ARF. In this case the transmission loss in nested tubes is of 0.055 dB/m at 1 THz. Finally, the solid green line corresponds to adjacent nested HC-ARF with 0.065 dB/m loss at 1 THz with a minimum loss of 0.055 dB/m at 1.05 THz. In these comparisons, the nested HC-ARF provides the lower transmission loss than regular HC-ARF and a smoother loss curve over the frequency regime than the adjacent nested HC-ARF. The small indentation of the adjacent nested tubes form the nodes near the core boundary and induce the loss peak in the transmission band due to Fano resonances [23], [24] at the lower frequency regime.

The oscillations in transmission band are more obvious when the adjacent nodes are positioned very close to the core boundary as shown in Fig. 2(b). The adjacent nested tube position is defined from the angle between the apex of adjacent tube and antiresonant tube as shown inset of Fig. 2(b). The adjacent node position of 40° offers improved transmission spectra over 60°, 90° and 120°.

Fig. 2(c) illustrates that the size and position of the adjacent nested tubes make little difference to the loss spectrum. In this simulation, we scan the distance between the adjacent nested tubes with constant antiresonant tube diameter from $z/D = 0.15$ to 0.25 for the adjacent node position of 40° and 90° and observe a small effect on the loss spectrum. However, the loss peaks are more obvious below 1 THz. The observation on size and position of the adjacent nested HC-ARF reduces the fabrication obligation.

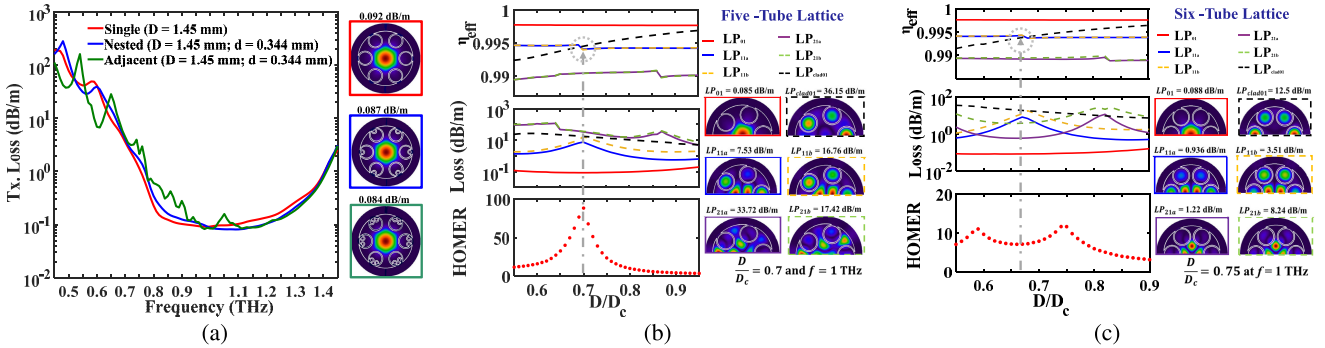

FIGURE 3. (a) Transmission loss of regular, nested, and adjacent nested ARF. The effect of changing inner tube diameter D on η_{eff}, loss, HOMER and mode field pattern for (b) five-tubes, and (c) six-tubes HC-ARF. All fibers have the same core diameter, $D_c = 3$ mm and uniform Zeonex strut thickness, $t = 0.09$ mm and $g = 0.99$ mm.

B. SIX-TUBE BASED HC-ARFs

As a comparison, we investigate the simulation results of six-tube HC-ARFs. It is important to mention that the previously reported HC-ARF have focused on six or more antiresonant tubes [22], [25], [28]–[31], [43]. Fig. 3(a) displays the calculated transmission loss spectra for the single, nested, adjacent nested six-tube HC-ARF. The red solid line indicates the single HC-ARF with a minimum loss of 0.092 dB/m. Blue and green lines are for the nested and adjacent nested HC-ARFs showing minimum transmission losses values 0.087 dB/m and 0.084 dB/m, respectively. All the losses are calculated at 1 THz. Fig. 3(a) demonstrate that the regular six-tube HC-ARF provides wider transmission spectra than the similar six-tube nested and adjacent nested HC-ARFs. The six-tube nested and adjacent nested HC-ARFs maintain the similar transmission spectra above 1.1 THz. Below 1.1 THz, the six-tube adjacent nested HC-ARF with node position of 40° provides a very small oscillation in the transmission spectra due to reduced Fano resonances. This Fano-induced oscillation is comparatively lower than the five-tube adjacent nested HC-ARF with node position of 90°, as previously demonstrated in Fig. 2(a-b). Moreover, the six-tube fibers with three different configurations show comparatively higher transmission loss and narrower transmission spectra than their equivalent five-tube geometries, as shown in Fig. 2(a).

C. HIGHER-ORDER MODE EXTINCTION RATIO

In this section, the modal properies of HC-ARFs are numerically analyzed with a fixed D_c, while the cladding tube diameter is varied over a range where the HOMs are suppressed at $f = 1$ THz. At this frequency, the lowest mode LP_{01} shows the smallest transmission loss and has become the dominant mode in HC-ARFs in this manuscript. In Fig. 3(b) and Fig. 3(c), the LP_{11a} and LP_{11b} shows almost similar refractive indices, therefore can be considered as first set of HOM, where modal intensity distribution are also identical. They are distinguished by electric field distribution as LP_{11a} and LP_{11b} (not shown in the Figure).

In order to investigate the coupling mechanism between the core and cladding modes, we carry out simulations as a function of D/D_c with constant D_c. Fig. 3(b) shows the characteristics of a five-tube lattice HC-ARF where it can be seen that the effective mode indices (η_{eff}) remains almost unchanged for all the core modes as a function of D/D_c. Interestingly, for a narrow range ($0.64 \leq D/D_c \leq 0.76$) the loss remains 0.09 dB/m, whereas D dominates the HOMs losses. The FM loss increases with D beyond $D/D_c \geq 0.77$. At $D/D_c = 0.7$, the modes (cladding and HOMs) strongly couple with each other therefore higher-order mode extinction ratio (HOMER) is obtained. Note that, the HOMER is used to quantitatively measure fibers single mode performance. It is defined as the ratio of core HOMs loss and FM loss [45], [46].

A similar calculation for the six-tube fiber, Fig. 3(c), shows that the FM loss can also be similar to the five-tube fiber however within a comparatively broader range ($0.55 \leq D/D_c \leq 0.76$) than that of five-tube fiber for the sack of lower HOMER. The maximum HOMs loss for LP_{11a} and LP_{11b} are obtained when $D/D_c \sim 0.68$. However, the LP_{21a} shows comparatively lower loss than the LP_{11} group from the range of $0.59 \leq D/D_c \leq 0.74$. As a result, a maximum HOMER of $\sim$11 is obtained at $D/D_c = 59$ and 75 respectively, that is lower than the five-tube fiber. However, a small separation (for example $D/D_c = 59$) between the antiresonant tubes leads to challenging fabrication of the fiber.

For further understanding the modal characteristics of the nested HC-ARF we show the transmission losses and HOMER by contour plottings that are shown in Fig. 4(a), from where it is possible to determine the single mode and low loss operating region of the fiber. Fig. 4a(ii), showing evident that, within $0.7 \leq D/D_c \leq 1.2$ and $0.3 \leq z/D \leq 0.73$ the loss of the FM maintains 0.05 dB/m. Fig. 4a(iii) indicates that maintaining the FM loss below 0.05 dB/m, the loss of HOMs can be high as 7.3 dB/m for $D/D_c = 1.09$ and $z/D = 0.34$. The loss in HOMs is high because of the strong coupling between the core HOMs and cladding modes [44]. Therefore, according to the obtained result it can

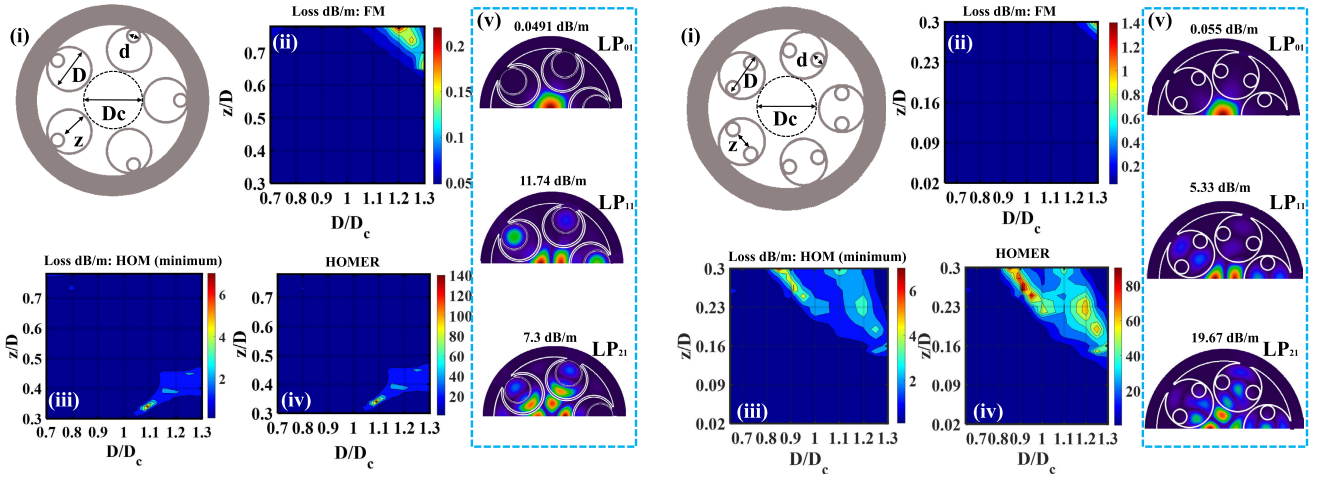

FIGURE 4. (a), (i) Cross section of the five-tube based nested ARF. The transmission loss of (ii) FM; (iii) HOMs, and (iv) HOMER. (v) Respective mode pattern of LP_{01}, LP_{11}, and LP_{21} at $D/D_c = 1.09$ and $z/D = 0.34$. (b), (i) Cross section of the five-tube based adjacent nested ARF. Calculated total transmission loss of (ii) FM; (iii) HOMs, and (iv) HOMER. (v) Respective mode pattern of LP_{01}, LP_{11}, and LP_{21} at $D/D_c = 0.91$ and $z/D = 0.26$. The simulations to plot this figure are performed at 1 THz, with $D_c = 3$ mm and $t = 0.09$ mm.

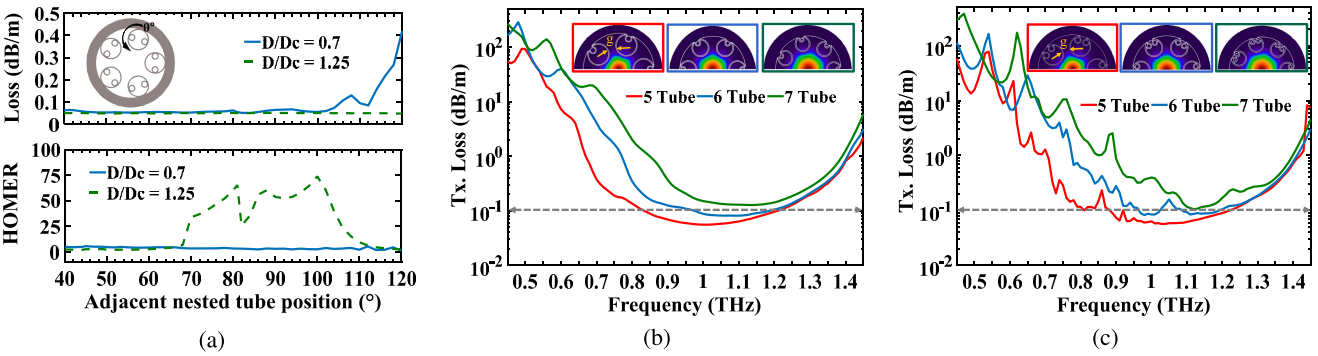

FIGURE 5. (a) Simulated transmission loss spectra and HOMER for five tube adjacent nested tube positions having $D/D_c = 0.7$ and $z/D = 0.2$. Calculated transmission losses of five, six and seven tube based, (b) regular nested and (c) adjacent nested fibers having $D/D_c = 0.7$. Note that, for (a-c) the optimum dimensions i.e $D_c = 3$ mm, $t = 0.09$ mm and $g = 0.99$ mm are chosen.

be said that, by engineering the antiresonant tubes the HOMs can be significantly suppressed.

The HOMER of the nested AR-HCFs is also investigated that is shown in Fig. 4a(iv). This indicates that a maximum HOMER of $>$ 140 can be obtained. To our knowledge, this is the highest HOMER value for any kind of terahertz fiber.

An extensive analysis of losses (FM and HOMs) and HOMER as a function of D/D_c and z/D for the angular position of their weld point at $\theta = 90°$ is also carried out, Fig. 4(b) that the results pertain to adjacent nested ARF. It can be seen that, for a wide range of z/D and D/D_c the FM loss remains constant where the minimum loss is 0.048 dB/m. However, due to relatively weak coupling between the HOMs and cladding modes, the HOMER is relatively small (slightly higher than 97).

The effect of changing adjacent nested tube positions on loss and HOMER is shown in Fig. 5(a). The change in adjacent nested tube position can also introduce the lower LP_{02} mode than LP_{11}, or LP_{21} in very limited cases. we also considered the losses of LP_{02} to calculate the HOMER. The loss and HOMER in calculated by keeping the, g, constant and changing the angular position, θ. We found that at $D/D_c = 0.7$, adjacent nested five-tube HC-ARF exhibits higher sensitivity to the modal contamination and behaves as a multimode waveguide. The weld position between 40° and 70° are more sensitive to HOMs and behaves as multi-mode (the ratio $D/D_c = 1.25$, $z/D = 0.2$). The achieved HOMER is ∼80 at $D/D_c = 1.25$ with weld position, $\theta = 100°$. The weld position $\theta = 90°$ provides HOM suppression of >57, adequate for single mode operation. However, The position at 40° generates less resonance than 60°, 90° and 120° (see also Fig. 2(b)). This is due to the core and nodes between adjacent nested tube in primary capillaries being further away from the core, as shown in Fig. 2(b).

D. EFFECT OF TUBE NUMBER ON TRANSMISSION LOSS

The effect of antiesonant tube numbers for constant adjacent tube gap on the transmission spectra is studied in this section. Both the nested and the adjacent nested HC-ARFs

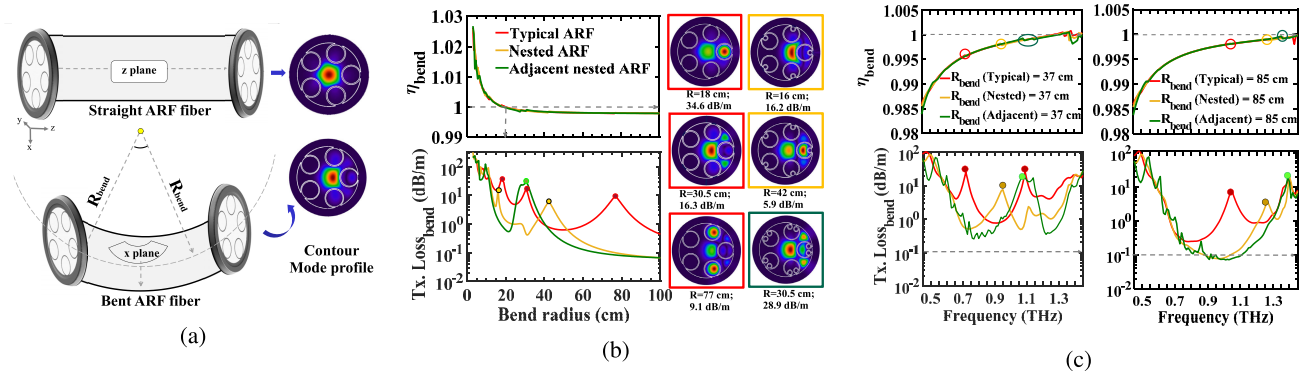

FIGURE 6. (a) Symbolic representation of straight and bent ARFs, and the corresponding LP_{01} modes. Calculated η_{bend} and transmission losses as a function of (b) bend radius (R_{bend}) at 1 THz and (c) frequency for five-tube typical, nested and adjacent nested ARFs. Note that, the optimum dimensions i.e $D_c = 3$ mm, $D/D_c = 0.7$, $t = 0.09$ mm, $d = 0.54$ mm, $z/D = 0.2$, $\theta = 40°$ and $g = 0.99$ mm are chosen.

are considered and analyzed for five, six and seven tubes. The transmission losses are shown in Fig. 5(b-c), where it is found that the five-tube nested and adjacent nested HC-ARF show similar transmission losses (0.055 dB/m at 1 THz and 0.056 dB/m at 1.03 THz, respectively) and wider transmission bandwidths as compared to the six and seven tubes. This is because of the larger distance from the core to the jacket for five-tube fibers. Generally the size of air regions inside the tube inversely related with the tube numbers. As the tube number increases the size of air regions decreases when the tube-gap is considered fixed. However, all the adjacent nested HC-ARFs with weld position 40° are influenced slightly with Fano-induced oscillations in the transmission band.

E. BENDING LOSSES

The total diameter of the proposed five-tube ARF is 9.56 mm (when $D/D_c = 0.7$) and can also be considered flexible compared to the flexible terahertz tube lattice fiber (9.6 mm) [25]. The flexible waveguides are deserved for terahertz imaging applications; however, the curvature of the fiber introduces bending loss. The bending loss of a fiber is characterized in two sequential forms: curvature dependent and frequency dependent confinement loss.

The curvature dependent bending loss starts with the transition of curvature radii from zero (and infinite for straight fiber) to finite (for bent fiber). Fig. 6(a) shows the schematic transition of straight ARF to bent ARF including the corresponding fundamental mode profiles respectively. The light propagates through the z-plane for both straight and bent fiber. The bending of straight fiber towards x-plane makes the fiber bent and deforms the fundamental air-core index profile LP_{01} towards the cladding tube. This deformation of index profile towards the cladding tube enhances the confinement loss as compared to straight fiber. The air-core index profile for the bent fiber, $\eta_{\text{bend}}(x)$ is quantified using the equation [25], [47], [48]

$$\eta_{\text{bend}}(x) = \eta(x) \exp \frac{x}{R_{\text{bend}}} \tag{1}$$

where $\eta(x)$ denotes a refractive index profile of straight fiber. In simulation, we use $\eta(x) = 1$. Here, x is the bending direction and R_{bend} defines the bend radius.

For analyzing the optical properties of bent fiber in Fig. 6(b) as a function of bend radius R_{bend}, we consider the five-tubes ARFs with three proposed structures as shown in Fig. 1. In Fig. 6(b), the optical properties are considered for $D_c = 3$ mm, $D/D_c = 0.7$ and $t = 0.09$ mm at 1 THz. We numerically analysis the η_{bend} and transmission loss of bent fiber by varying the R_{bend} between 3 cm to 100 cm. The smaller the R_{bend} the greater the curvature of the fiber, which highly deforms the desired air-core index profile LP_{01} towards the cladding tube. Light leakages from the air-core through the gap, g and the phase match between LP_{01} and LP_{clad01} are responsible for $\eta_{\text{bend}} \geq 1$ when $R_{\text{bend}} \leq 20$. For ease of visualization, we include the air-core index profile LP_{01} according to the cladding structures in Fig. 6(b). Also, we numerically analyze the transmission loss of the bent fiber, which is known to affect bending loss. The bending loss spectra for the three structures introduce undesired high loss peaks over the range of R_{bend}. The high loss peaks arises in bent fiber when higher mode contamination and phase matching between core and cladding modes become dominant. With $D/D_c = 0.7$, the bending losses differ due to the cladding pattern variations. The regular ARF shows a higher loss region with more pronounced peaks than nested and adjacent nested fiber. The high loss peaks of 34.6, 16.3 and 9.1 dB/m for regular ARFs appear around $R_{\text{bend}} = 18$, 30.5 and 85 cm respectively. The high loss peaks in nested ARFs appear around $R_{\text{bend}} = 16$, and 42 cm with the bending loss of 16.2 dB/m and 5.9 dB/m respectively. The adjacent nested ARF shows a high loss of 28.9 dB/m around $R_{\text{bend}} = 30.5$ cm. Excluding the high loss peak, adjacent nested ARF shows comparatively lower loss between the $R_{\text{bend}} = 3$ and 80 cm than regular and nested ARFs. Both the nested and adjacent nested ARFs shows similar loss spectra when $R_{\text{bend}} \geq 80$ cm. Next, we investigate the frequency dependent refractive indices and bending losses for five-tube ARFs; comparatively with small and large bend radius,

R_{bend} = 37 and 85 cm as shown in Fig. 6(c). The η_{bend} in regular, nested and adjacent nested for R_{bend} = 37 and 85 cm follow the similar trends over the frequency range between 0.45 and 1.45 THz. The disruptions of η_{bend} marked with circles cause high losses peaks. For example, regular ARFs with R_{bend} = 37 cm causes high loss peaks of 25 dB/m around 0.72 and 1.09 THz. The adjacent nested ARFs with R_{bend} = 37 cm offers a lower loss of 0.26 dB/m at 0.77 THz than the nested fiber. The regular ARF suffers from the bending loss and narrower transmission region than the nested and adjacent nested ARFs. The adjacent nested and nested ARFs carry the same bending loss of 0.07–0.09 dB/m around 1.01 THz for the large bend radius, R_{bend} = 85 cm. Also, the adjacent nested ARF shows a slightly broader transmission bandwidth than the nested ARF. However, the bending loss curve for adjacent ARF is not as smooth as regular and nested bending loss curve because of the reduced Fano resonance introduced from the adjacent node of angle 40°. As a comparison between two bend radii, the frequency dependent bending loss for R_{bend} = 37 cm shows more pronounced peaks and higher loss than the R_{bend} = 85 cm in Fig. 6(c) due to the small bend radius. The smaller the R_{bend}, the higher the bending loss.

Finally, the impact of antiresonant tube numbers using a fixed adjacent gap is analyzed to investigate the bending loss and HOMER as a function of R_{bend} in Fig. 7. The effective refractive index for five tubes is higher than six and seven tubes. This results in a small refractive index variation between the LP_{01} and LP_{clad01} of five antiresonant tubes. As a result, when the five-tube ARF is bent in the xz plane the LP_{clad01} and LP_{01} are easily phased matched at small bend radii and the higher-order mode becomes dominant. The bending loss for five-tube nested ARF is higher than seven tubes and six tubes at $R_{bend} \leq 24$ cm and $24 \leq R_{bend} \leq 75$ respectively. Similar results are obtained for seven and six-tube adjacent nested ARF at $R_{bend} \leq 16$ cm and $23 \leq R_{bend} \leq 65$ respectively. Surprisingly, the five-tube nested and adjacent nested ARFs at $R_{bend} \geq 75$ cm and $R_{bend} \geq 65$ cm provide lower loss than six and seven-tube ARFs. The bending loss for large bend radii and straight fiber maintains a similar concept, for example, five tubes offers lower loss as larger antiresonant tubes allow phase matching between the LP_{clad01} and lowest HOM, making the LP_{01} dominant. The most achievable lowest HOM includes the LP_{11}, LP_{21}, LP_{02}. The seven tubes in large bend radii and straight fiber provide the highest loss due to the short core-cladding distance using a constant adjacent tube gap.

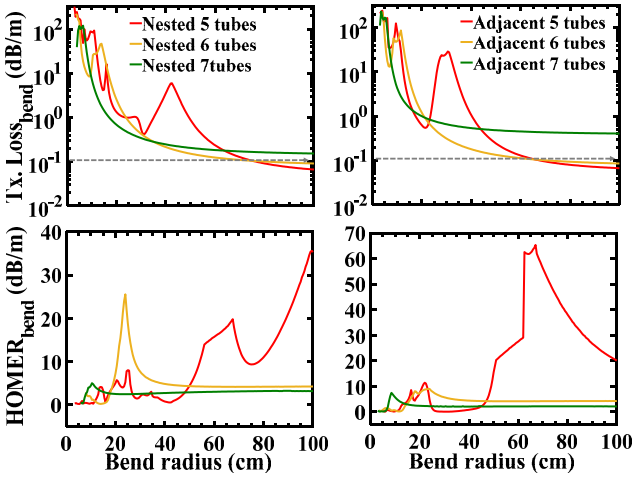

FIGURE 7. (a) Calculated transmission losses and HOMER of five, six and seven tube based on regular nested and adjacent nested fibers having $D/D_c = 0.7$. Note that, the optimum dimensions i.e $D_c = 3$ mm, $D/D_c = 0.7$, $t = 0.09$ mm, $d = 0.54$ mm, $z/D = 0.2$, $\theta = 40°$, $g = 0.99$ mm and $f = 1$ THz are chosen.

For bent fiber with nested and adjacent nested tubes, we attempt to show the HOMER (ratio between lowest HOM and LP_{01}) in Fig. 7 when the adjacent tube gap, g is constant. The five- tube ARFs are bend sensitive than six and seven tubes and can achieve comparatively larger HOMER for large bend radii. The both five and six-tube nested ARFs can provide HOMER at large and small bend radius respectively. However, the five-tube adjacent nested ARF achieves the highest HOMER of 65 at $D/D_c = 0.7$, $\theta = 40°$ and $f = 1$ THz. The mode contamination appears in six and seven-tube adjacent nested bent ARFs.

IV. CONCLUSION

We propose three different cladding structures with typical single, regular nested, and adjacent nested HC-ARFs. We systematically analyse these designs by varying D/D_c with a constant gap separation, g. To find the best performing fiber, more investigations are carried out systematically on z/D, adjacent nested tube angle, and spacing. We find that the five-tube HC-ARF exhibits lower loss and wider transmission bandwidths as compared to six and seven tube designs. Also regular nested HC-ARF are not susceptible to Fano resonances as is the case for adjacent nested HC-ARFs, and provide a superior HOM suppression of 140. It is important to note that the five-tube ARFs are bend sensitive and suffer from higher bending loss for small bend radii than six and seven tubes. Also, the small bend radius shrinks the transmission window.

REFERENCES

[1] B. Ferguson and X.-C. Zhang, "Materials for terahertz science and technology," *Nature Mater.*, vol. 1, no. 1, pp. 26–33, Sep. 2002.

[2] M. Tonouchi, "Cutting-edge terahertz technology," *Nature Photon.*, vol. 1, no. 2, pp. 97–105, Feb. 2007.

[3] B. S. Williams, "Terahertz quantum-cascade lasers," *Nature Photon.*, vol. 1, no. 9, pp. 517–525, 2007.

[4] M. S. Islam, J. Sultana, A. Dinovitser, M. Faisal, M. R. Islam, B. W.-H. Ng, and D. Abbott, "Zeonex-based asymmetrical terahertz photonic crystal fiber for multichannel communication and polarization maintaining applications," *Appl. Opt.*, vol. 57, no. 4, pp. 666–672, 2018.

[5] M. S. Islam, J. Sultana, K. Ahmed, M. R. Islam, A. Dinovitser, B. W.-H. Ng, and D. Abbott, "A novel approach for spectroscopic chemical identification using photonic crystal fiber in the terahertz regime," *IEEE Sensors J.*, vol. 18, no. 2, pp. 575–582, Jan. 2018.

[6] M. S. Islam, J. Sultana, A. A. Rifat, A. Dinovitser, B. W.-H. Ng, and D. Abbott, "Terahertz sensing in a hollow core photonic crystal fiber," *IEEE Sensors J.*, vol. 18, no. 10, pp. 4073–4080, Mar. 2018.

[7] W. L. Chan, J. Deibel, and D. M. Mittleman, "Imaging with terahertz radiation," *Rep. Progr. Phys.*, vol. 70, no. 8, pp. 1325–1379, Jul. 2007.
[8] D. Mittleman, *Sensing With Terahertz Radiation*. Cham, Switzerland: Springer, 2003.
[9] K. Wang and D. M. Mittleman, "Metal wires for terahertz wave guiding," *Nature*, vol. 432, no. 7015, pp. 376–379, Nov. 2004.
[10] T. Ito, Y. Matsuura, M. Miyagi, H. Minamide, and H. Ito, "Flexible terahertz fiber optics with low bend-induced losses," *J. Opt. Soc. Amer. B, Opt. Phys.*, vol. 24, no. 5, pp. 1230–1235, 2007.
[11] L.-J. Chen, H.-W. Chen, T.-F. Kao, J.-Y. Lu, and C.-K. Sun, "Low-loss subwavelength plastic fiber for terahertz waveguiding," *Opt. Lett.*, vol. 31, no. 3, pp. 308–310, 2006.
[12] A. Hassani, A. Dupuis, and M. Skorobogatiy, "Low loss porous terahertz fibers containing multiple subwavelength holes," *Appl. Phys. Lett.*, vol. 92, no. 7, Feb. 2008, Art. no. 071101.
[13] M. S. Islam, S. Rana, M. R. Islam, M. Faisal, H. Rahman, and J. Sultana, "Porous core photonic crystal fibre for ultra-low material loss in THz regime," *IET Commun.*, vol. 10, no. 16, pp. 2179–2183, Nov. 2016.
[14] K. Nielsen, H. K. Rasmussen, P. U. Jepsen, and O. Bang, "Porous-core honeycomb bandgap THz fiber," *Opt. Lett.*, vol. 36, no. 5, pp. 666–668, Mar. 2011.
[15] J. Anthony, R. Leonhardt, S. G. Leon-Saval, and A. Argyros, "THz propagation in Kagome hollow-core microstructured fibers," *Opt. Express*, vol. 19, no. 19, pp. 18470–18478, Sep. 2011.
[16] T.-I. Jeon, J. Zhang, and D. Grischkowsky, "THz sommerfeld wave propagation on a single metal wire," *Appl. Phys. Lett.*, vol. 86, Mar. 2005, Art. no. 161904.
[17] S. Atakaramians, S. Afshar V., T. M. Monro, and D. Abbott, "Terahertz dielectric waveguides," *Adv. Opt. Photon.*, vol. 5, no. 2, pp. 169–215, Jun. 2013.
[18] M. S. Islam, J. Sultana, C. M. B. Cordeiro, A. L. S. Cruz, A. Dinovitser, B. W.-H. Ng, and D. Abbott, "Broadband characterization of glass and polymer materials using THz-TDS," in *Proc. 44th Int. Conf. Infr., Millim., Terahertz Waves (IRMMW-THz)*, Sep. 2019, pp. 1–2.
[19] J.-Y. Lu, C.-P. Yu, H.-C. Chang, H.-W. Chen, Y.-T. Li, C.-L. Pan, and C.-K. Sun, "Terahertz air-core microstructure fiber," *Appl. Phys. Lett.*, vol. 92, no. 6, Feb. 2008, Art. no. 064105.
[20] L. Vincetti, "Numerical analysis of plastic hollow core microstructured fiber for terahertz applications," *Opt. Fiber Technol.*, vol. 15, no. 4, pp. 398–401, Aug. 2009.
[21] D. S. Wu, A. Argyros, and S. G. Leon-Saval, "Reducing the size of hollow terahertz waveguides," *J. Lightw. Technol.*, vol. 29, no. 1, pp. 97–103, Jan. 1, 2011.
[22] L. Vincetti, V. Setti, and M. Zoboli, "Terahertz tube lattice fibers with octagonal symmetry," *IEEE Photon. Technol. Lett.*, vol. 22, no. 13, pp. 972–974, Apr. 19, 2010.
[23] L. Vincetti and V. Setti, "Fano resonances in polygonal tube fibers," *J. Lightw. Technol.*, vol. 30, no. 1, pp. 31–37, Jan. 1, 2012.
[24] L. Vincetti and V. Setti, "Extra loss due to Fano resonances in inhibited coupling fibers based on a lattice of tubes," *Opt. Express*, vol. 20, no. 13, pp. 14350–14361, 2012.
[25] V. Setti, L. Vincetti, and A. Argyros, "Flexible tube lattice fibers for terahertz applications," *Opt. Express*, vol. 21, no. 3, pp. 3388–3399, 2013.
[26] E. Arrospide, G. Durana, M. Azkune, G. Aldabaldetreku, I. Bikandi, L. Ruiz-Rubio, and J. Zubia, "Polymers beyond standard optical fibres-fabrication of microstructured polymer optical fibres," *Polym. Int.*, vol. 67, no. 9, pp. 1155–1163, 2018.
[27] S. Atakaramians, S. A. V, H. Ebendorff-Heidepriem, M. Nagel, B. M. Fischer, D. Abbott, and T. M. Monro, "THz porous fibers: Design, fabrication and experimental characterization," *Opt. Express*, vol. 17, no. 16, pp. 14053–14062, Jul. 2009.
[28] W. Lu, S. Lou, X. Wang, Y. Shen, and X. Sheng, "Demonstration of low-loss flexible fiber with zeonex tube-lattice cladding for terahertz transmission," in *Proc. Opt. Fiber Commun. Conf.*, 2015, doi: 10.1364/OFC.2015.M3D.2.
[29] M. M. Nazarov, A. V. Shilov, K. A. Bzheumikhov, Z. C. Margushev, V. I. Sokolov, A. B. Sotsky, and A. P. Shkurinov, "Eight-capillary cladding THz waveguide with low propagation losses and dispersion," *IEEE Trans. THz Sci. Technol.*, vol. 8, no. 2, pp. 183–191, Mar. 2018.
[30] A. L. S. Cruz, V. A. Serrão, C. L. Barbosa, M. A. R. Franco, C. M. de Barros Cordeiro, A. Argyros, and X. Tang, "3D printed hollow core fiber with negative curvature for terahertz applications," *J. Microw. Optoelectron. Electromagn. Appl.*, vol. 14, pp. SI-45–SI-53, Jul. 2015.
[31] L. D. van Putten, J. Gorecki, E. N. Fokoua, V. Apostolopoulos, and F. Poletti, "3D-printed polymer antiresonant waveguides for short-reach terahertz applications," *Appl. Opt.*, vol. 57, no. 14, pp. 3953–3958, 2018.
[32] G. K. M. Hasanuzzaman, S. Iezekiel, C. Markos, and M. S. Habib, "Hollow-core fiber with nested anti-resonant tubes for low-loss THz guidance," *Opt. Commun.*, vol. 426, pp. 477–482, Nov. 2018.
[33] F. Gérôme, R. Jamier, J.-L. Auguste, G. Humbert, and J.-M. Blondy, "Simplified hollow-core photonic crystal fiber," *Opt. Lett.*, vol. 35, no. 8, pp. 1157–1159, Apr. 2010.
[34] A. N. Kolyadin, A. F. Kosolapov, A. D. Pryamikov, A. S. Biriukov, V. G. Plotnichenko, and E. M. Dianov, "Light transmission in negative curvature hollow core fiber in extremely high material loss region," *Opt. Express*, vol. 21, no. 8, pp. 9514–9519, 2014.
[35] F. Poletti, "Nested antiresonant nodeless hollow core fiber," *Opt. Express*, vol. 22, no. 20, pp. 23807–23828, 2014.
[36] P. Uebel, M. C. Günendi, M. H. Frosz, G. Ahmed, N. N. Edavalath, J.-M. Ménard, and P. S. J. Russell, "Broadband robustly single-mode hollow-core PCF by resonant filtering of higher-order modes," *Opt. Lett.*, vol. 41, no. 9, pp. 1961–1964, 2016.
[37] M. Michieletto, J. K. Lyngsø, C. Jakobsen, J. Lægsgaard, O. Bang, and T. T. Alkeskjold, "Hollow-core fibers for high power pulse delivery," *Opt. Express*, vol. 24, no. 7, pp. 7103–7119, 2016.
[38] C. Wei, R. J. Weiblen, C. R. Menyuk, and J. Hu, "Negative curvature fibers," *Adv. Opt. Photon.*, vol. 9, no. 3, pp. 504–561, 2017.
[39] M. I. Hasan, N. Akhmediev, and W. Chang, "Positive and negative curvatures nested in an antiresonant hollow-core fiber," *Opt. Lett.*, vol. 42, no. 4, pp. 703–706, 2017.
[40] S.-F. Gao, Y.-Y. Wang, X.-L. Liu, W. Ding, and P. Wang, "Bending loss characterization in nodeless hollow-core anti-resonant fiber," *Opt. Express*, vol. 24, no. 13, pp. 14801–14811, 2016.
[41] M. S. Habib, O. Bang, and M. Bache, "Low-loss hollow-core silica fibers with adjacent nested anti-resonant tubes," *Opt. Express*, vol. 23, no. 13, pp. 17394–17406, Jun. 2015.
[42] W. Belardi and J. C. Knight, "Hollow antiresonant fibers with low bending loss," *Opt. Express*, vol. 22, no. 8, pp. 10091–10096, 2014.
[43] L. Vincetti and V. Setti, "Waveguiding mechanism in tube lattice fibers," *Opt. Express*, vol. 18, no. 22, pp. 23133–23146, 2010.
[44] A. Argyros and J. Pla, "Hollow-core polymer fibres with a kagome lattice: Potential for transmission in the infrared," *Opt. Express*, vol. 15, no. 12, pp. 7713–7719, 2007.
[45] M. S. Habib, O. Bang, and M. Bache, "Low-loss hollow-core anti-resonant fibers with semi-circular nested tubes," *IEEE J. Sel. Topics Quantum Electron.*, vol. 22, no. 2, pp. 156–161, Mar. 2016.
[46] M. S. Habib, J. E. Antonio-Lopez, C. Markos, A. Schülzgen, and R. Amezcua-Correa, "Single-mode, low loss hollow-core anti-resonant fiber designs," *Opt. Express*, vol. 27, no. 4, pp. 3824–3836 2019.
[47] H. Bao, K. Nielsen, O. Bang, and P. U. Jepsen, "Dielectric tube waveguides with absorptive cladding for broadband, low-dispersion and low loss THz guiding," *Sci. Rep.*, vol. 5, no. 1, Jul. 2015, Art. no. 7620.
[48] H. Li, S. Atakaramians, R. Lwin, X. Tang, Z. Yu, A. Argyros, and B. T. Kuhlmey, "Flexible single-mode hollow-core terahertz fiber with metamaterial cladding," *Optica*, vol. 3, no. 9, pp. 941–947, Sep. 2016.

JAKEYA SULTANA received the B.Sc. (Eng.) degree from the Rajshahi University of Engineering and Technology and the M.Sc. degree in engineering from the Islamic University of Technology, Bangladesh, in 2014 and 2017, respectively. She is currently pursuing the Ph.D. degree with the School of Electrical and Electronic Engineering, The University of Adelaide, Australia. Her research interests include antiresonant fibers for terahertz applications and super-continuum generation. She is an active Reviewer of the IEEE JOURNAL OF LIGHTWAVE TECHNOLOGY, the IEEE PHOTONIC TECHNOLOGY LETTERS, *Optik*, and *Optics Communications*.

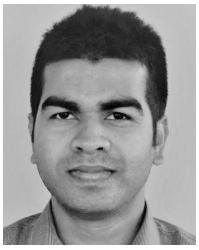

MD. SAIFUL ISLAM (Member, IEEE) is currently pursuing the Ph.D. degree with the School of Electrical and Electronic Engineering, The University of Adelaide, Australia. He has published 43 peer-reviewed articles. His research interests include optical fiber communication, PCF-based terahertz waveguides, terahertz sensors, surface plasmon resonance biosensors, topological insulators, and metamaterials for sensing applications. He is a member of the IEEE Young Professionals, Optical Society of America (OSA), and Institute for Photonics and Advanced Sensing (IPAS). He received a top peer reviewer in physics and cross-fields, in 2019, as recognized by Publons and Web of Science. He is an actively Reviews of *Scientific Reports*, *Photonics Research*, the IEEE JOURNAL OF LIGHTWAVE TECHNOLOGY, the IEEE PHOTONICS JOURNAL, the IEEE SENSORS JOURNAL, the IEEE PHOTONICS TECHNOLOGY LETTERS, *Optics Express, Applied Optics, Optical Materials Express,* and *Optical Fiber Technology*.

CRISTIANO M. B. CORDEIRO received the Ph.D. degree from the University of Campinas (UNICAMP), Brazil. He held a postdoctoral position at the University of Bath, England. He is currently an Assistant Professor with the Institute of Physics, UNICAMP, and the Head of the Specialty Optical Fiber Laboratory. He is the author of 70 journal publications, 50 communications in international conferences, a book chapter, and eight patents. The main research areas of the laboratory are the development and application of silica photonic crystal fibers, microstructured polymer optical fibers, and micro/nanofibers. His topics of interest include exploring new fiber functionalities and the use of new technologies in the optical fiber area. Applications related with optical devices and fiber sensors are under investigation. He Chaired the first Workshop on Specialty Optical Fibers (WSOF), which is now in its sixth cycle.

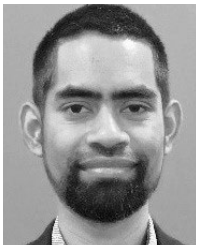

MD. SELIM HABIB (Senior Member, IEEE) received the B.Sc. and M.Sc. degrees in electrical and electronic engineering from the Rajshahi University of Engineering and Technology, Rajshahi, Bangladesh, in 2008 and 2012, respectively, and the Ph.D. degree in photonics engineering from the Technical University of Denmark (DTU), in 2017. After finishing his Ph.D., he joined as a Postdoctoral Researcher at the Fibers Sensors and Supercontinuum Group, Department of Photonics Engineering, DTU. After finishing his Postdoctoral Fellowship at DTU, he worked as a Postdoctoral Research Associate at CREOL, The College of Optics and Photonics, University of Central Florida, USA, from September 2017 to August 2019. He is currently an Assistant Professor of electrical and computer engineering with Florida Polytechnic University, USA. He has published more than 40 articles in refereed journals. His research mainly focuses on design, fabrication, and characterization of low loss hollow-core fiber in the near-IR to mid-IR, light gas nonlinear interaction in hollow-core fibers, supercontinuum generation, and multi-mode nonlinear optics. He is an Optical Society of America (OSA) Early Careers Member and an Executive officer of OSA Fiber modeling and Fabrication group. He received the University Gold Medal Award from the Rajshahi University of Engineering and Technology, in 2014. He is an Associate Editor of IEEE ACCESS and *Feature Editor of Applied Optics* (OSA).

ALEX DINOVITSER (Member, IEEE) is currently a Postdoctoral Fellow with The University of Adelaide, Australia. He has worked within the electronics manufacturing industry, and designing computer interface and signal acquisition systems. In 2008, he built the first spectroscopic lidar in Australia for the differential absorption detection of atmospheric trace gasses. He is also a member of the Optical Society of America (OSA) and Engineers Australia.

BRIAN WAI-HIM NG (Member, IEEE) is currently a Senior Lecturer with the School of Electrical and Electronic Engineering, The University of Adelaide. His research interests include radar signal processing, wavelets, and terahertz (T-ray) signal processing. He was awarded the University of Adelaide Medal for the Top Graduate in Electrical and Electronic Engineering. He is currently an active member with the South Australian Chapter of the IEEE.

DEREK ABBOTT (Fellow, IEEE) was born in South Kensington, London, U.K., in 1960. He received the B.Sc. (Hons.) degree in physics from Loughborough University, Leicestershire, U.K., in 1982, and the Ph.D. degree in electrical and electronic engineering from The University of Adelaide, Australia, in 1995, under K. Eshraghian and B. R. Davis. His interests are in the area of multidisciplinary physics and electronic engineering applied to complex systems. His research programs span a number of areas of stochastics, game theory, photonics, energy policy, biomedical engineering, and computational neuroscience. He is a Fellow of the Institute of Physics, U.K., and an Honourary Fellow of Engineers Australia. He has won a number of awards, including the South Australian Tall Poppy Award for Science, in 2004, the Premier's SA Great Award in Science and Technology for outstanding contributions to South Australia, in 2004, an Australian Research Council Future Fellowship, in 2012, the David Dewhurst Medal, in 2015, the Barry Inglis Medal, in 2018, and the M. A. Sargent Medal, in 2019. He has served as an Editor and/or Guest Editor for a number of journals, including the IEEE JOURNAL OF SOLID STATE CIRCUITS, *Journal of Optics B*, *Microelectronics Journal*, *Chaos*, *Smart Structures and Materials*, *Fluctuation and Noise Letters*, the PROCEEDINGS OF THE IEEE, and the IEEE PHOTONICS JOURNAL. He has served on the Editorial Board of the PROCEEDINGS OF THE IEEE, from 2009 to 2014, the Editorial Board of IEEE ACCESS, since 2015, and since 2019, he has been serving on the IEEE Publications Publication Services and Products Board (PSPB).